Compensation for Dynamic Subdivision Error When the Grating Displacement Sensor Code Disk Is Stained

Changhai Zhao, *Member, IEEE*, Qiuhua Wan, and Lihui Liang

***Abstract*—When the code disk of a displacement sensor gains dust or other impurities, its moiré fringe signal will deviate from the standard range, which increases subdivision error. In this study, a high-speed A/D converter was used to collect the moiré fringe signal of a sensor in real time and to extract the characteristic points. The center point trajectory of the moiré fringe signal Lissajous figure was calculated, and the amplitude values of the two moiré fringe signals were determined according to characteristic points. The moiré fringe signals according to the center point trajectory and signal amplitudes were then normalized. Error compensation of the dc level and amplitude of moiré fringe signals was realized, so as to improve the dynamic subdivision accuracy of moiré fringe signals when the code disk was stained. Experiments showed that, when the reading head was in the stained area of the code disk, the subdivision error of moiré fringe signals was reduced from the peak value of 37.2″ to 4.6″, and the accuracy of the sensor can be improved using this algorithm for both different resolutions and different stains, which greatly improved the ability of the displacement sensor to adapt to a harsh environment.**

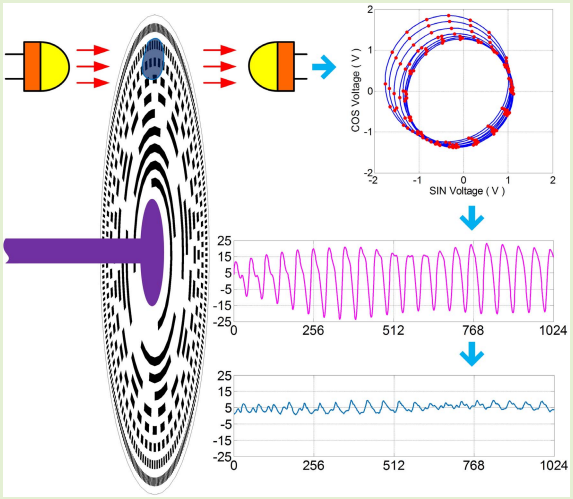

***Index Terms*—Characteristic points, error compensation, grating, stain, subdivision error.**

I. Introduction

AT PRESENT, various high-precision displacement measurement systems using grating moiré fringe subdivision technology are the main means for obtaining displacement information [1], [2], [3]. Due to the limited technical level of grating engraving accuracy, equipment manufacturing, assembly, and adjustment technology, as well as the inherent diffraction characteristics of light, high-precision and high-resolution measurements are difficult to achieve with displacement sensors only by manufacturing higher precision grating code disks. Current common practice is to use moiré fringe subdivision technology to improve the resolution and accuracy of displacement sensors, with the quality of grating moiré fringe signals closely related to sensor the accuracy [4], [5], [6], [7].

Ideally, moiré fringe signal output from the grating of a displacement sensor comprises two orthogonal sine-wave signals. However, due to the manufacturing and assembly process, actual signal output is a quasi-sine-wave signal, which has a certain deviation from a standard sine-wave signal [8], [9], [10], [11], [12]. Subdividing the moiré fringe signal based on the standard sine wave will inevitably lead to subdivision error. For a high-precision displacement sensor, subdivision error is the main source of its error. At present, the general method for improving the accuracy of a displacement sensor is through error compensation. For example, a method has been developed involving taking the average of multiple reading heads to improve sensor accuracy. Full cycle sampling, taking the high-precision displacement sensor as the benchmark, error measuring of each position of the sensor, and then error compensation have all been used to improve sensor accuracy. An alternative method is to collect the sensor moiré fringe signal and use Fourier analysis to calculate signal harmonics. Then, the signal subdivision error is calculated according to the harmonic characteristics and the subdivision error compensated to improve the displacement sensor

Manuscript received 28 August 2022; revised 25 December 2022; accepted 25 December 2022. Date of publication 4 January 2023; date of current version 31 January 2023. This work was supported in part by the National Natural Science Foundation of China under Grant 52075520 and in part by the Science and Technology Development Program of Jilin Province under Grant 20210201097GX. The associate editor coordinating the review of this article and approving it for publication was Dr. Varun Bajaj. *(Corresponding author: Changhai Zhao.)*

The authors are with the Changchun Institute of Optics, Fine Mechanics and Physics, Chinese Academy of Sciences, Changchun 130033, China (e-mail: zhaoch@ciomp.ac.cn).

Digital Object Identifier 10.1109/JSEN.2022.3232708

subdivision accuracy. The above methods can improve sensor accuracy to a certain extent [13], [14], [15], [16], [17]. However, when a displacement sensor runs for a period of time or experiences external environmental changes, its moiré fringe signal parameters will change. At this point, the subdivision error of the moiré fringe signal changes. If the traditional compensation algorithm is used to compensate for sensor error, the compensation effectiveness is greatly reduced and sometimes counterproductive. In particular, when the displacement sensor is used in harsh environments, its code disk might suffer from condensation or other stains, with the stained degree and area of the code disk changing at any time. When the reading head of the sensor moves to the stained area, the moiré fringe signal will change dramatically. At this time, the traditional error compensation algorithm is powerless. When the sensor subdivision error becomes too large, the displacement sensor will be miscoded, resulting in the sensor being unusable.

The amplitude and dc level errors of a sensor moiré signal are the main components of interpolation error. When the external environment changes or when the sensor code disk is stained, the dc level and amplitude of the moiré fringe signal will be affected. In this study, a high-speed, high-precision A/D converter was used to collect sensor moiré fringe signals in real time. Taking the sampling points with uniformly distributed slopes on the moiré fringe signal Lissajous figure as characteristic points, the dc level and amplitude of the moiré signal were calculated, and the dc level and amplitude errors are then compensated. When the sensor was in motion, one signal characteristic point was updated for every 1/16th of a moiré fringe signal period. This algorithm for error compensating the signal was independent of sensor motion parameters. When the sensor worked normally, with sensor movement of the sensor, real-time compensation of dc level and amplitude errors was realized. When the moiré fringe signal changed due to external environmental changes or staining of the code disk, the proposed algorithm greatly reduced signal subdivision error, and the real-time error compensation was strong. This greatly improved the ability of the displacement sensor to adapt to the external environment and enhanced sensor reliability.

II. Subdivision of Moiré Fringe Signal

A. Signal Characteristics of Moiré Fringe

The principle of displacement sensor subdivision is derived from the equation $\tan\theta = \sin\theta/\cos\theta$, in which θ is the theoretical value of the subdivision angle and $\sin\theta$ and $\cos\theta$ the two orthogonal precise code moiré fringe signals under ideal conditions. Calculation of precise code moiré fringe signal subdivisions of a displacement sensor was performed using the following equation:

$$\theta = \tan^{-1}\left(\frac{\sin\theta}{\cos\theta}\right). \tag{1}$$

In a high-precision displacement sensor, sensor accuracy is mainly determined by the subdivision accuracy of the precise code moiré fringe signal and the error source mainly from the subdivision error of the fringe [18], [19], [20]. Subdivision error is expressed by the phase difference, which is the difference between the actual subdivision point phase and the theoretical subdivision point phase, expressed as follows:

$$d\theta = \varphi - \theta = \tan^{-1}\left(\frac{u_a}{u_b}\right) - \tan^{-1}\left(\frac{\sin\theta}{\cos\theta}\right) \tag{2}$$

where $d\theta$ is the subdivision error of the displacement sensor, $\varphi = \tan^{-1}((u_a/u_b))$ the actual subdivision point phase, and $\theta = \tan^{-1}((\sin\theta/\cos\theta))$ the theoretical subdivision point phase.

Here, $\sin\theta$ and $\cos\theta$ are two theoretical signals from the displacement sensor, comprised of two ideal sine waves with a phase difference of 90°, and U_a and U_b the two grating moiré fringe signals of the actual displacement sensor. There is a certain deviation between them and the standard sinusoidal signal, which is expressed by a Fourier series, expressed as follows:

$$\begin{cases} U_a = a_0 + a_1 \cdot \sin(\theta + \phi) + \sum_{i=2}^{\infty} a_i \cdot \sin\left(i\theta + \phi_{i_a}\right) + \delta_e \\ U_b = b_0 + b_1 \cdot \cos(\theta + \phi_b) + \sum_{i=2}^{\infty} b_i \cdot \cos(i\theta + \phi_{ib}) + \delta_e. \end{cases} \tag{3}$$

Each Fourier expression contains four subexpressions, where a_0 and b_0 are the direct components of the signal, which are sources of dc component error; a_1 and b_1 the amplitudes of the fundamental signals, which are sources of signal amplitude error; ϕ and ϕ_b the fundamental phases of U_a and U_b, with the phase difference of the two signals of the source of phase error; $\sum_{i=2}^{\infty} a_i \cdot \sin(i\theta + \phi_{ia})$ and $\sum_{i=2}^{\infty} b_i \cdot \cos(i\theta + \phi_{ib})$the sum of higher harmonic components, which are sources of harmonic component error; and δ_e the electrical noise, which is the source of noise error. When the photoelectric displacement sensor stays at a certain position, the theoretical voltage output by the sensor moiré fringe signal should be $\sin\theta$ and $\cos\theta$, but the voltage of the actual output signal is U_a and U_b, as shown in (3), which inevitably produces subdivision error.

B. Calculation of Subdivision Error

Each reading head of the displacement sensor has four light-emitting elements and four photoelectric receiving elements. The light emitted by the light-emitting elements is irradiated on the photoelectric receiving elements through the code disk and the slit. The photoelectric receiving element outputs four original moiré fringe signals with a phase difference of 90°, which are J0, J90, J180, and J270, respectively. The J0 and J180 signals with a phase difference of 180° pass through the differential amplifier and become sine signal (SIN), namely, U_a; similarly, the J90 and J270 signals with a phase difference of 180° pass through the differential amplifier and become cosine signal (COS), namely, U_b. When the displacement sensor is used for a period of time, the external environment can change or stains can appear on the code disk, and the transmittance of the code disk will change, resulting in

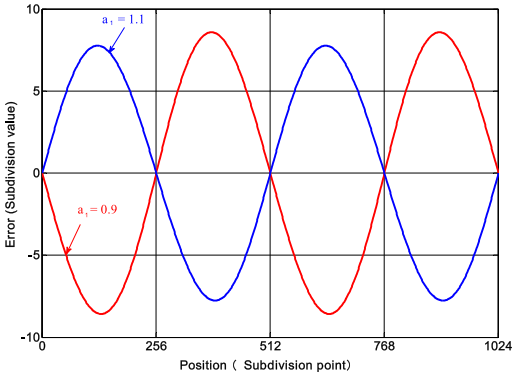

Fig. 1. Error curve when amplitudes not the same.

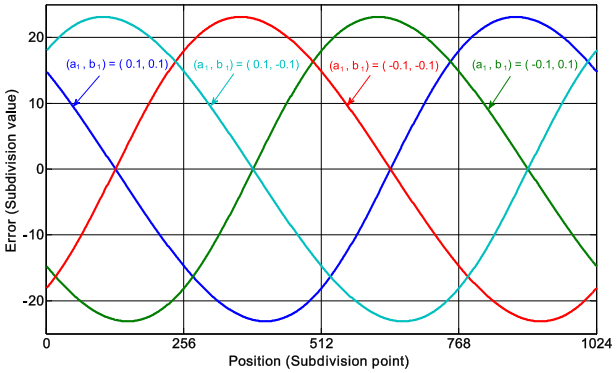

Fig. 2. Subdivision error curve with dc level.

insufficient optical signal received by the photoelectric receiving element, and the current signal output by the receiving element will be smaller than the normal current signal. The moiré fringe signal output by the sensor will deviate from its initial signal. Because the shape of the stain is not fixed, the attenuation amplitude of the four receiving element signals will be inconsistent. The main parameters affected are the dc level and amplitude of the signal, which leads to increased subdivision error. When the subdivision error reaches a certain value, sensor bit error will be caused, and the sensor cannot be used.

When the amplitude of two moiré fringe signals from the sensor increases or decreases by the same multiple at the same time (1), the subdivision value of the signal will not be affected, and there will be no subdivision error at this time. However, in actual use, the amplitude changes of the two moiré fringe signals are generally not the same. When the two signals only have amplitude errors, assuming that the amplitude of the cos θ signal is 1 and the amplitude of the sin θ signal is a_1, the signal expression at this time was as shown in the following equation:

$$\begin{cases} U_a = a_1 \cdot \sin(\theta) \\ U_b = \cos(\theta). \end{cases} \tag{4}$$

The subdivision error curve of the moiré fringe signal calculated by (2) in one subdivision period, when a_1 is a different value, is shown in Fig. 1. For convenience of calculation, a period of a precise code moiré fringe signal of the sensor was subdivided into 10 bits, that is, 1024 data points, and the unit of subdivision error a bit.

When there is only a dc level error in the two moiré fringe signals, the signals represented in the following equation are expressed as follows:

$$\begin{cases} U_a = a_0 + \sin(\theta) \\ U_b = b_0 + \cos(\theta). \end{cases} \tag{5}$$

When a_0 and b_0 are different values, the subdivision error curves of the moiré fringe signal calculated by (2) in one subdivision period are shown in Fig. 2.

When the moiré fringe signal has both amplitude and dc level errors, the resulting subdivision error curve is the superposition of the curves in Figs. 1 and 2.

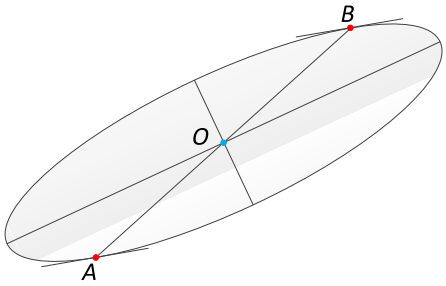

Fig. 3. Lissajous figure after filtering out high-order harmonics.

III. Error Compensation Algorithm

A. Lissajous Figure Characteristics

The Lissajous figure is the synthetic trajectory of two sinusoidal vibrations along mutually perpendicular directions. When analyzing the actual signal of a displacement sensor, the Lissajous figure is often used to analyze sensor error. The Lissajous figure formed by the two completely orthogonal sine and COSs is a standard circle. When debugging the actual sensor, the subdivision error of the moiré fringe is estimated by observing the Lissajous figure deviation from the standard circle and the accuracy of the sensor determined regarding meeting design requirements.

When the external environment changes, the dc level and amplitude of the moiré fringe signal are mainly affected, with less impact on the higher harmonics. In actual calculations, the higher harmonics of the moiré fringe signal are considered fixed values and error compensation of the higher harmonics realized using a fixed error compensation table. After the sensor is manufactured, or when accuracy needs to be calibrated, the sensor is rotated at a constant speed to collect a complete moiré fringe signal cycle of the displacement sensor. Each harmonic of the signal is obtained by Fourier calculation. After filtering out dc level and amplitude errors, the subdivision error of each subdivision point is calculated using (2) and then stored in nonvolatile flash memory in the form of an error data table. When calculating sensor displacement, the difference between the subdivision value actually calculated and the value in the error data table is the precise code subdivision value after compensation.

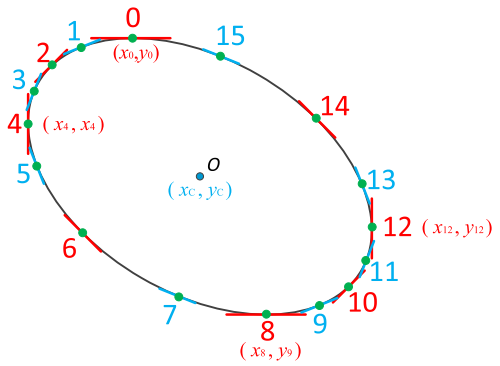

Fig. 4. Sixteen characteristic points of Lissajous figure.

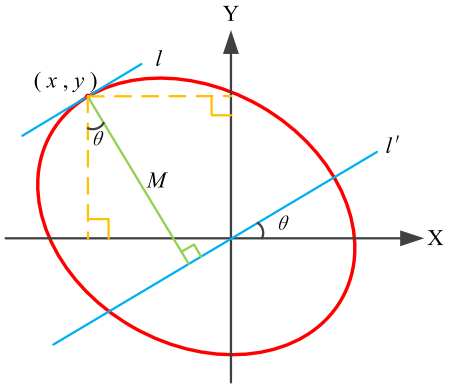

Fig. 5. Calculation of coordinate of characteristic points in Lissajous figure.

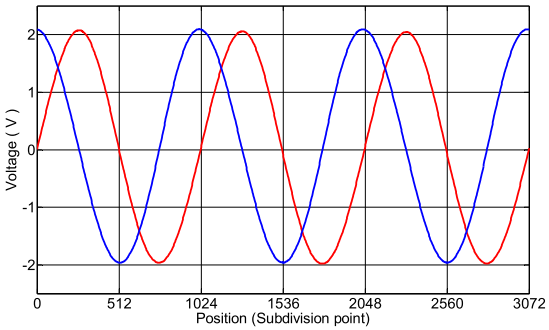

Fig. 6. Two moiré fringe signals.

After filtering out higher harmonics, the expression of the moiré fringe signal is shown in (6) and its Lissajous figure in Fig. 3.

Because $\sin\theta = -\sin(\theta + \pi)$ and $\sin\theta = -\sin(\theta + \pi)$, the Lissajous figure is a central symmetric figure with point $O(a_0, b_0)$ as the central point. A line segment composed of two points tangent to the Lissajous figure by two parallel lines at any angle, and the midpoint of the line segment is the center point of the Lissajous figure (Fig. 3, line segment AB). The difference between the peak and valley values of the abscissa was twice the amplitude a_1 of U_a, and similarly, the difference between the peak and valley values of the ordinate coordinate was twice the amplitude b_1 of U_b

$$\begin{cases} U_a = a_0 + a_1 \cdot \sin(\theta + \phi) \\ U_b = b_0 + b_1 \cdot \cos(\theta + \phi_b). \end{cases} \tag{6}$$

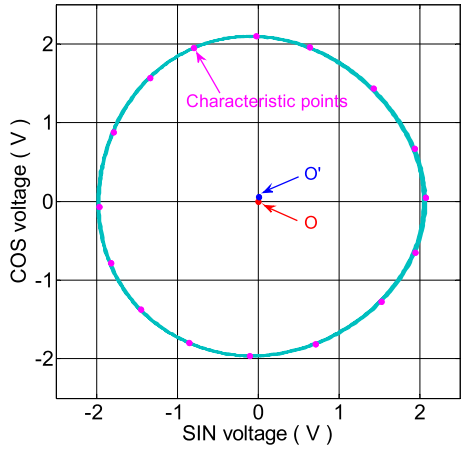

Fig. 7. Lissajous figure from clean code disk.

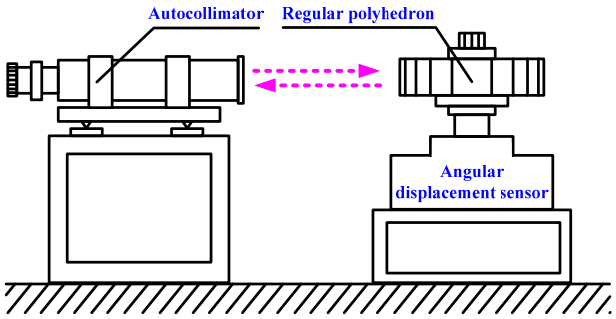

Fig. 8. Schematic of static subdivision error measurement.

B. Center Point Calculation

When the displacement sensor moves, if the code disk is clean and the external environment does not change, the sensor outputs a stable moiré fringe signal. The Lissajous figure is similar to that shown in Fig. 3, with the center point fixed and coordinates of the center point and signal amplitude easily calculated, thus realizing error compensation for the dc level and amplitude of the signal.

When the external environment changes sharply or there are stains on the code disk, the moiré fringe signal output by the sensor is an unstable signal and the center point of the Lissajous figure also unstable. Because the motion parameters of the sensor were unpredictable in actual work, it was impossible to accurately calculate the coordinates of its center point and only approximate coordinates of its center point calculated.

In this study, the coordinates of 16 characteristic points on the Lissajous figure were taken as benchmarks (Fig. 4). The Lissajous figure and point tangent to the line with an angle of $(n\pi/8)$ on the X-axis were used as characteristic points, where $n = 0, 1, \ldots, 15$. Taking the average value of 16 coordinate points as the center point of the Lissajous figure and according to the center point coordinates, the dc level of the moiré fringe signal was calculated.

When the sensor was actually moving, the Lissajous figure collected discrete data and, theoretically, the point tangent to the figure could not be accurately obtained. In actual calculations, the maximum calculated value was taken as the

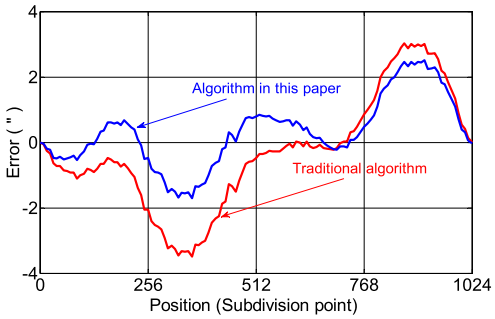

Fig. 9. Subdivision error curve from clean code disk.

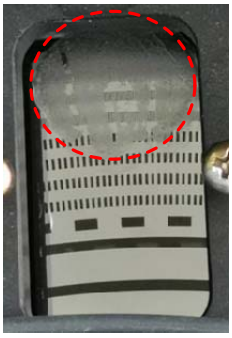

Fig. 10. Code disk water stain image.

tangent point, according to collected data points and calculation equation (Fig. 5). When calculating the point where the straight line l was tangent to the Lissajous circle, only the sampling value of the moiré fringe signal needed to be substituted into (7) to calculate its peak data point, which was saved as the characteristic point of the Lissajous figure

$$M = y \cdot \cos\theta - x \cdot \sin\theta \tag{7}$$

where (x, y) is the coordinate of the data point on the Lissajous figure, which is the voltage value of two moiré fringe signals; θ the angle between line l and X-axis; M the distance from the point on the Lissajous figure to the vertical line segment of line l'; and l' the line parallel to l and passing through the origin of the coordinate system.

When the sensor was moving, moiré fringe signal data were collected in real time and the data judged whether a characteristic point according to the equation for each characteristic point. When the collected Lissajous data point matched one of the 16 characteristic points, the data of the characteristic point were updated. The calculation of each characteristic point of the Lissajous figure was the peak data obtained by (7), in which $\theta = (n\pi/8)$ $n = 0, 1, \ldots, 15$.

When the sensor moved for a complete precise coding cycle, all characteristic point data were updated. When calculating the coordinates of characteristic points, the system had no special requirements for the motion state of the sensor. When the sensor motion speed was too fast and the sampling speed insufficient, data for some characteristic points collected were inaccurate. The actual test showed that, when sampling data points of each moiré fringe signal cycle were more than 32, the collected characteristic point data met the needs of system accuracy.

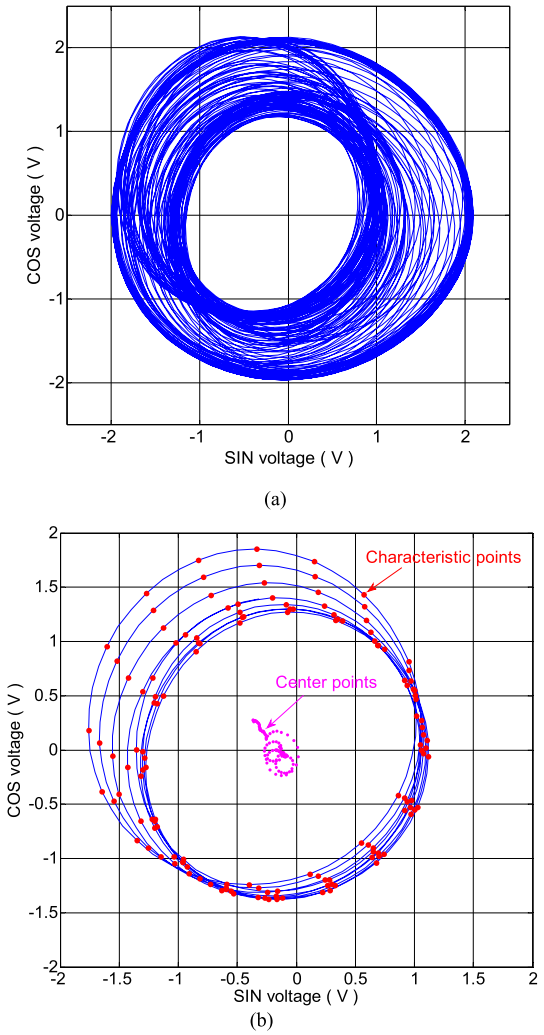

Fig. 11. Lissajous figure when code disk is stained. (a) Lissajous figure when the reading head passes through stained area from nonstained area of code disk. (b) Lissajous figure when reading head in stained area.

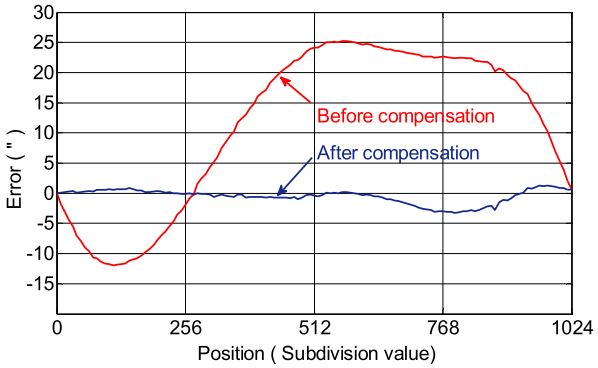

Fig. 12. Static subdivision error curve from stained code disk, with position where moiré fringe signal subdivision value at 0 used as measurement starting point.

C. Error Compensation

Assuming that the coordinate values of the 16 characteristic points of the Lissajous figure were (x_n, y_n) and $n = 0$–15, then the coordinates of the center point (x_C, y_C) of the Lissajous

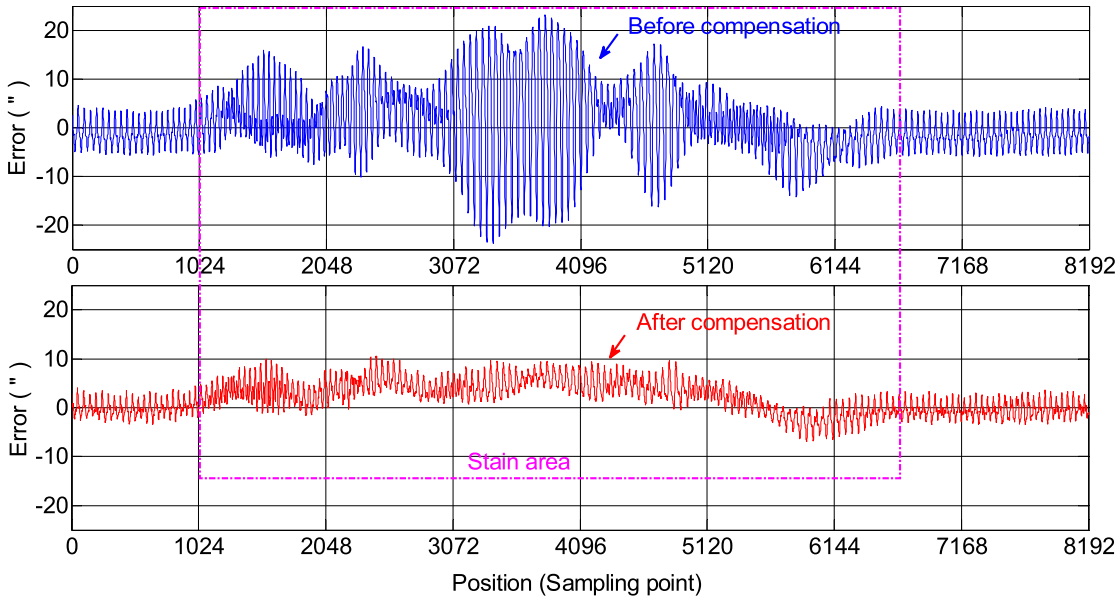

Fig. 13. Dynamic subdivision error curve when the reading head passes through stained area of code disk.

Fig. 14. Code disk stain figure.

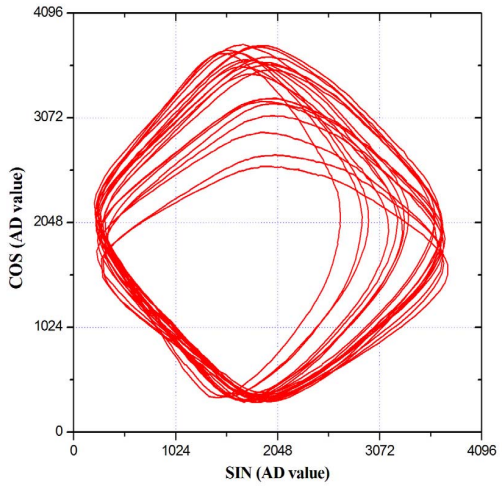

Fig. 15. Lissajous figure when the code disk is stained.

figure were calculated using the following equation:

$$\begin{cases} x_C = \dfrac{1}{16} \cdot \sum_{i=0}^{15} x_i \\ y_C = \dfrac{1}{16} \cdot \sum_{i=0}^{15} y_i. \end{cases} \tag{8}$$

When the Lissajous figure center was obtained, the figure was divided into four quadrants according to the coordinate value of the center point. Each quadrant corresponded to its own signal amplitude value, according to which the two original collected moiré fringe signals were normalized. If the voltage values of the fringe signal before normalization were U_a and U_b, then the signal voltages after normalization were U_a' and U_b'. From these, the calculations of the first to fourth quadrants were performed using the following equations:

$$\begin{cases} U'_a = \dfrac{u_a - x_C}{x_{12} - x_C} \\ U'_b = \dfrac{u_b - y_C}{y_0 - y_C} \end{cases} \tag{9}$$

$$\begin{cases} U'_a = \dfrac{u_a - x_C}{x_C - x_4} \\ U'_b = \dfrac{u_b - y_C}{y_0 - y_C} \end{cases} \tag{10}$$

$$\begin{cases} U'_a = \dfrac{u_a - x_C}{x_C - x_4} \\ U'_b = \dfrac{u_b - y_C}{y_C - y_8} \end{cases} \tag{11}$$

$$\begin{cases} U'_a = \dfrac{u_a - x_C}{x_{12} - x_C} \\ U'_b = \dfrac{u_b - y_C}{y_C - y_8}. \end{cases} \tag{12}$$

According to the normalized voltage values of the two moiré fringe signals, the sensor displacement value was calculated using (1), so as to realize the error compensation of the dc level and amplitude of the signal. When using this algorithm for error compensation, as the center point of the Lissajous graph and signal amplitude value could change at any time, a small range of jumps might be caused in the output displacement value. In the precise code subdivision, the actual subdivision bits were 2–3 bits higher than the output effective bits,

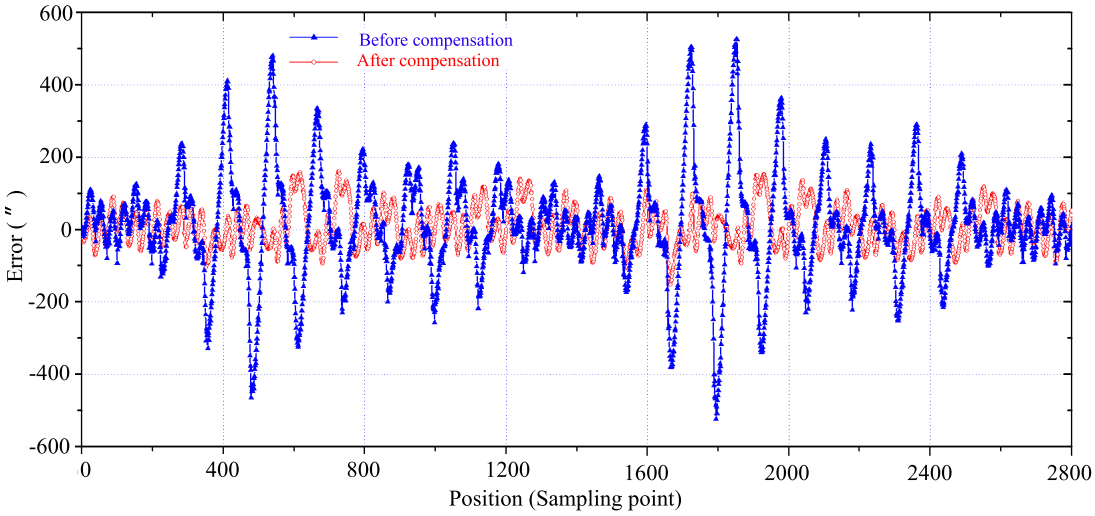

Fig. 16. Error curve of sensor before and after compensation.

which ensured continuity of the sensor output displacement value.

IV. Experiment

Taking a 22-bit angular displacement sensor as the experimental object, the number of precise coding lines of the angular displacement sensor was 4096 lines/cycle and the corresponding angle of each precise coding cycle at 316.40625″. A 12-bit A/D converter was used to collect two-channel precise code moiré fringe signals from each reading head. Each precision code cycle was subdivided to 12 bits or 4096 pieces of data, with the highest sensor resolution reaching 24 bits. The continuity of output data was ensured by having the actual output of effective bits by the angular displacement sensor at 22 bits and the output subdivision bits at 10 bits.

When the external environment was stable, the code disk of the angular displacement sensor clean, and the displacement sensor rotated, the two moiré fringe signals output by the sensor reading head were observed and the Lissajous figure formed by them stable (Figs. 6 and 7, respectively). The center point coordinate from the 16 characteristic points of the Lissajous figure, at O'(0.0094, 0.0526), was very close to the center point of the coordinate system, at O(0,0).

The static accuracy measurement principle of the angular displacement sensor showed that, when measuring, the angular displacement sensor and regular polyhedron were coaxially connected. When the sensor was rotated, the autocollimator and regular polyhedron were used as angle references (Fig. 8). The difference between the angle display value of the displacement sensor and the angle value of the regular polyhedron was the static error of the displacement sensor at the measuring point. Then, with continued sensor rotation, all test points were observed, thus completing the test. Using the traditional algorithm and this algorithm, the subdivision error curve was drawn (Fig. 9). When the sensor code disk was clean and the environment stable, the traditional algorithm was used, resulting in peak and valley values of the static subdivision error at 3.0″ and −3.5″ and the mean square error 1.7″. When this algorithm was used, the peak and valley values of the static subdivision error were 2.5″ and −1.7″ and the mean square error 1.0″. Using this algorithm significantly improved the accuracy of the displacement sensor.

The actual working conditions of the sensor in the field were simulated. When water stains were introduced on the code disk of the angular displacement sensor (Fig. 10), the Lissajous figure and its characteristic points and center points were determined (Fig. 11). Taking one subdivision period of the stained area of the disk as the measurement object, the traditional and the present algorithms were used and the static subdivision error curves determined (Fig. 12). When the code disk was stained, the output Lissajous figure was unstable. With the traditional algorithm, the peak value of static subdivision error was 25.2″, the valley value −12.0″, and mean square error 13.16″. When using this compensation algorithm, the peak value of static subdivision error was 1.3″, the valley value −3.3″, and mean square error 1.19″. Using this algorithm significantly reduced the subdivision error caused by a code disk stain.

When the displacement sensor rotated and its reading head passed through the stained area of the code disk, its dynamic subdivision error curve was observed (Fig. 13). The present algorithm was found to reduce the subdivision error caused by the stain. When the sensor worked in speed mode, the effects after compensation were particularly clear. The compensation algorithm in this article is carried out automatically when the sensor is working. When the code disk of the sensor is not stained, the difference between the displacement value after compensation and that before compensation is very small. When the code disk of the displacement sensor is stained, the subdivision error after compensation will be greatly reduced. Using the present algorithm, thus, improved the ability of the displacement sensor to adapt to harsh environments.

Due to the limited resolution of A/D conversion in this system, when using this algorithm, it is necessary to ensure that the sensor can output the moiré fringe signal normally and the amplitude value of the signal cannot be too small. When there is stain on the code disk, if the amplitude value of the moiré fringe signal output by the sensor is greater than

one eighth of the standard amplitude value, the system can still output 22-bit effective angle value. When the signal amplitude value is less than one eighth of the standard value, the effective resolution of the sensor output will be reduced, and only the number of bits can be reduced during use. For example, it is used as a 20-bit sensor.

Take a 16-bit small angular displacement sensor as another example, the sensor fine code number is 256 lines per cycle; using a 12-bit A/D converter to collect two moiré fringe data, one fine code moiré fringe signal cycle corresponds to an angle of 5062.5″. When the code disk of the displacement sensor is stained, as shown in Fig. 14, the Lissajou figure formed is shown in Fig. 15.

The error curve of displacement sensor before and after compensation is shown in Fig. 16. The peak and valley error values of the sensor before compensation were 526″ and −523″, and the peak and valley error values of the sensor after compensation were 160″ and −152″. From Figs. 13 and 16, it can be seen that the accuracy of the sensor can be improved by using this algorithm for different resolutions and different stains.

V. Conclusion

In this study, a method for extracting 16 characteristic points of the Lissajous figure from the displacement sensor was used to calculate the coordinates of the figure center point. This allowed real-time compensation for errors from dc level and amplitude values of the precise code of the sensor, which, thus, improved sensor accuracy. The present algorithm was simple and took a subdivision period of the stained area of the code disk as the measurement object. When the code disk of the displacement sensor was stained and this algorithm used for subdivision, the peak and valley values of static subdivision error were reduced from 37.2″ to 4.6″ and mean square error reduced from 13.16″ to 1.19″, and the accuracy of the sensor can be improved using this algorithm for both different resolutions and different stains, thus greatly improving the ability of the displacement sensor to adapt to harsh environments.

References

[1] N. Wang, W. Jiang, and Y. Zhang, "Deep learning-based Moiré-fringe alignment with circular gratings for lithography," *Opt. Lett.*, vol. 46, no. 5, pp. 1113–1116, Mar. 2021.

[2] M. Li et al., "Large-scale range diffraction grating displacement sensor based on polarization phase-shifting," *Appl. Opt.*, vol. 59, no. 2, pp. 469–473, Jan. 2020.

[3] G. Zhao et al, "Electronic interpolation interface based on linear subdivision method for sinusoidal optical encoders," *IEEE Sensors J.*, vol. 20, no. 7, pp. 3646–3654, Apr. 2020.

[4] Y. Lee, S. H. Kim, S.-H. Lee, and C. C. Chung, "Encoder calibration method for high precision servo systems with a sinusoidal encoder," *IEEE Trans. Ind. Electron.*, vol. 69, no. 1, pp. 752–762, Jan. 2022.

[5] P. Yuan, D. Huang, and Z. Lei, "An improved high-precision subdivision algorithm for single-track absolute encoder using machine vision techniques," *Meas. Control*, vol. 52, nos. 5–6, pp. 675–686, Apr. 2019.

[6] W. Zhang, Y. Wang, H. Du, Q. Zeng, and X. Xiong, "High-precision displacement measurement model for the grating interferometer system," *Opt. Eng.*, vol. 59, no. 4, Apr. 2020, Art. no. 045101.

[7] W. Zhu, S. Ye, Y. Huang, and Z. Xue, "Design of a precise subdivision system for gratings using a modified CORDIC algorithm," *IET Circuits, Devices Syst.*, vol. 13, no. 8, pp. 1284–1291, Nov. 2019.

[8] A. Jin, J. Lin, B. Liu, L. Wang, and P. Jin, "Moiré fringes-based measurement of radial error motion of high-speed spindle," *Opt. Lasers Eng.*, vol. 150, Mar. 2022, Art. no. 106852.

[9] G. Ye, G. Zhao, H. Liu, and B. Lu, "Precise phase demodulation algorithm for sinusoidal encoders and resolvers," *IEEE Trans. Ind. Electron.*, vol. 67, no. 10, pp. 8778–8787, Oct. 2020.

[10] G. Ye et al., "Ratiometric-linearization-based high-precision electronic interpolator for sinusoidal optical encoders," *IEEE Trans. Ind. Electron.*, vol. 65, no. 10, pp. 8224–8231, Oct. 2018.

[11] M. Abolhassani, "Sampling Moiré method using non-sinusoidal grating," *Optik*, vol. 231, Apr. 2021, Art. no. 166337.

[12] W. Zhu, Y. Xu, Y. Huang, Z. Xue, and S. Ye, "Subdivision method for nonorthogonal Moiré signals," *IEEE Trans. Instrum. Meas.*, vol. 70, pp. 1–10, 2021.

[13] J. Thomas, T. R. Rajanna, and S. Asokan, "Temperature compensated FBG displacement sensor for long-range applications," *IEEE Sensors Lett.*, vol. 4, no. 1, pp. 1–4, Jan. 2020.

[14] C. Chen, F. Mao, and J. Yu, "Subpixel sampling Moiré method for in-plane displacement measurement considering the symmetric errors induced by interpolation," *Appl. Opt.*, vol. 60, no. 5, pp. 1232–1240, Feb. 2021.

[15] L. Wang, Y. Wu, Y. Zhang, and S. Hao, "Research on angle subdivision method of multi-pole magnetic encoder based on pole number quotient remainder," *IEEE Trans. Magn.*, vol. 57, no. 10, pp. 1–12, Oct. 2021.

[16] W. Zhu, S. Ye, Y. Huang, and Z. Xue, "An improved CORDIC for digital subdivision of Moiré signal," *Metrol. Meas. Syst.*, vol. 27, no. 1, pp. 51–64, Mar. 2020.

[17] X. Gao, S. Li, and Q. Ma, "Subdivided error correction method for photoelectric axis angular displacement encoder based on particle swarm optimization," *IEEE Trans. Instrum. Meas.*, vol. 69, no. 10, pp. 8372–8382, Oct. 2020.

[18] C. Zhao, Q. Wan, X. Lu, and L. Liang, "Moiré fringe signal subdivision system of a stained code disc of a grating displacement sensor," *IEEE Sensors J.*, vol. 22, no. 9, pp. 8614–8621, May 2022.

[19] D. Gurauskis, A. Kilikevicius, and S. Borodinas, "Experimental investigation of linear encoder's subdivisional errors under different scanning speeds," *Appl. Sci.*, vol. 10, no. 5, p. 1766, Mar. 2020.

[20] W. Zhu, Y. Lin, Y. Huang, and Z. Xue, "Research on sinusoidal error compensation of Moiré signal using particle swarm optimization," *IEEE Access*, vol. 8, pp. 14820–14831, 2020.

Changhai Zhao (Member, IEEE) received the Ph.D. degree from the Changchun Institute of Optics, Fine Mechanics and Physics (CIOMP), Chinese Academy of Sciences, Changchun, China, in 2008.

He is currently an Associate Research Fellow with the CIOMP, Chinese Academy of Sciences. His research interests include the area of electro-optical displacement precision measurement.

Qiuhua Wan was born in 1962.

She is currently a Research Fellow with the Changchun Institute of Optics, Fine Mechanics and Physics (CIOMP), Chinese Academy of Sciences, Changchun, China. Her research interests include the area of electro-optical displacement precision measurement.

Lihui Liang was born in 1980.

He is currently an Associate Research Fellow with the Changchun Institute of Optics, Fine Mechanics and Physics (CIOMP), Chinese Academy of Sciences, Changchun, China. His research interests include the area of electro-optical displacement precision measurement.